CrossMark

ORIGINAL PAPER

Biosilica from sea water diatoms algae—electrochemical impedance spectroscopy study

Andrzej P. Nowak[1] · **Anna Lisowska-Oleksiak[1]** · **Beata Wicikowska[1]** ·
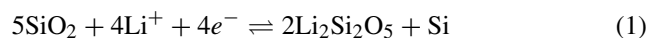**Maria Gazda[2]**

Abstract Here, we report on an electrochemical impedance study of silica of organic origin as an active electrode material. The electrode material obtained from carbonized marine biomass containing nanoporous diatoms has been characterised by means of XRD, IR, SEM and EIS. Different kinds of crystallographic phases of silica as a result of thermal treatment have been found. The electrode is electrochemically stable during subsequent cyclic voltammetry measurements taken in the potential range from 0.005 up to 3.0 V vs. Li/Li$^+$. The material has been found to exhibit high charge capacitance of 521 mAh g^{-1} being cycled at a rate C/20 with capacity retention of about 97%. Electrochemical impedance spectroscopy performed at an equilibrated potential $E = 0.1$ V in the temperature range 288–294 K discloses low charge transfer resistivity and low diffusional impedance.

✉ Andrzej P. Nowak
andnowak@pg.gda.pl

1 Faculty of Chemistry, Department of Chemistry and Technology of Functional Materials, Gdańsk University of Technology, Narutowicza 11/12, 80-233 Gdańsk, Poland

2 Faculty of Applied Physics and Mathematics, Gdańsk University of Technology, Narutowicza 11/12, 80-233 Gdańsk, Poland

Introduction

Carbon materials of different kinds and morphologies are used as anodes in lithium-ion batteries, mainly due to their plausible theoretical capacity (372 mAh g^{-1}) and good cycling performance [39]. However, the practical capacity is 300–320 mAh g^{-1}. Research towards a more efficient material in respect to storage capacity is still ongoing. There is a need to come up with a cheaper and more stable anode material [29].

Silicon, due to its high theoretical capacity of about 4200 mAh g^{-1} is considered as a replacement for graphite anodes in energy storage devices. The problem with practical usage of a silicon anode is that Si undergoes significant volume changes during alloying with lithium [33]. This pulverization process leads to contact loss of anode materials, resulting in capacity fading. Moreover, huge volume changes influence the mechanical stress of the electrode seen as degradation of the solid electrolyte interphase (SEI) layer and further capacity fading [6]. Recently, the silicon oxide nanostructures were tested as an alternative anode material for lithium batteries [5, 9, 32, 40]. Silica is one of the most commonly occurring matters on Earth. Silica as an anode material exhibits a high theoretical capacity of about 1965 mAh g^{-1} and is known to undergo faradaic processes in the presence of lithium ions at a sufficiently high cathodic potential. Yan et al. expressed the mechanism on the basis of HRTEM and SAED data as follows [40]:
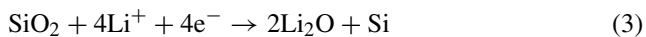
$$5SiO_2 + 4Li^+ + 4e^- \rightleftharpoons 2Li_2Si_2O_5 + Si \tag{1}$$

$$Si + xLi^+ + xe^- \rightleftharpoons Li_x Si \tag{2}$$

The two reactions are all reversible. However, Guo proposed a different mechanism with irreversible silicate formation and parallel lithium oxide creation [16]:

$$SiO_2 + 4Li^+ + 4e^- \rightarrow 2Li_2O + Si \tag{3}$$

$$2SiO_2 + 4Li^+ + 4e^- \rightarrow Li_4SiO_4 + Si \tag{4}$$
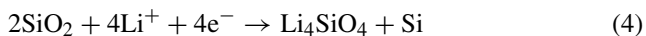
Above electrochemical reactions of SiO_2 can be the source of a high theoretical capacity, significantly higher than the capacity of LiC_6 [40]. Formation of disilicate in reaction (1), as also silicon lithiation (reaction (2)), are reversible; however, reactions (3) and (4) are found to be irreversible. In our previous study on an anode material obtained from high temperature transformation of sea water diatoms, we showed that under lithiation reversible, reactions took place. The tested material was a composite of the carbonaceous part and silica. Both parts of the active anode (carbonaceous part and silica) originated from carbonized biomass [23].

In this work, we focus on silica activity only while the carbonaceous part of the biomass was removed in the carbonization process (see Experimental part for details). It is due to the fact that there is a huge amount of natural resources, namely diatomic earth, available all around the world. Here, we use marine red algae covered with diatoms as a source of silica nanostructure. The marine biomass was collected in the southern part of the Baltic sea in the Gulf of Gdańsk. All material from red algae was chemically removed and only the part coming from diatoms has been used for anode preparation.

Electrochemical performance of silica anodes, of diatomic origin, has been studied by means of electrochemical impedance spectroscopy (EIS). EIS is one of the most powerful techniques used to investigate electrochemical behaviour of materials [12, 18, 26, 30, 35, 36, 38, 41]. It permits disclosing of different phenomena related to charge transfer and transport within the electrode material and at the electrode/electrolyte interface. Here, EIS has been used to characterise the material after cathodic polarisation at different temperatures.

Experimental

Marine algae (*Polysiphonia fucoides*) covered by diatoms (*Diatomophyceae*) from the Baltic Sea were cleaned mechanically (manually, ultrasonic bath) and chemically. After mechanical cleaning, algae were chemically cleaned by shaking in 1 M HCl solution for 24 h, followed by shaking in 1 M NaOH solution to remove excess of HCl and finally washed with distilled water. Next, the biomass was carbonized in a furnace (Czylok, Poland) at 900 °C for 2 h under a carbon dioxide flow of 20 ml min^{-1}. We used CO_2 as a mild oxidizing agent able to remove the organic part from the biomass. After pyrolysis, pure biosilica was milled for 1 h at 1500 rpm (Retsch, MM200, Germany).

The electrodes were prepared from a slurry (50 wt% of active material, 30 wt% of carbon black (Super P, Timcal, Switzerland) and 20 wt% of binder (polyvinylidene fluoride PVdF, Sole, Germany) in NMP on a 10-μm thin copper foil (Schlenk Metallfolien GmbH & Co KG, Germany). After tape casting, drying at 100 °C for 8 h, discs were cut from the tape and pressed (30 s with a load of 200 MPa). Next, the discs were dried under dynamic vacuum in an oven (Glass Oven B-585 Büchi, Germany) for 24 h at 80 °C and were used in two-electrode Swagelok® cells with lithium foil (99.9% purity, 0.75 mm thickness, AlfaAesar) as counter and reference electrodes with 1 M LiPF$_6$ in EC : DMC ratio 1 : 1 (LP30 Merck, Germany) as the electrolyte, and glass fibre (Schleicher & Schüll, Germany) as the separator.

The crystal structure of carbonized algae was determined from X-ray diffraction patterns (XRD) measured in the range of $2\theta = 20$–$80°$, using an X-ray diffractometer (Xpert PRO-MPD, Philips with copper K radiation ($\lambda = 1.5404$ Å).

The infrared spectrum was obtained on a Genesis II FTIR spectrometer (λ accuracy $\pm$ 2 cm^{-1}) in the range 400–2000 cm^{-1}. Samples were prepared as KBr pressed pellets.

EIS measurements were performed using a Frequency Response Analyser (FRA) module equipped Autolab PGSTAT 10 at a rest potential of 0.10 V. The three-electrode Swagelok® cells with lithium foil (99.9% purity, 0.75 mm thickness, AlfaAesar) as counter and lithium wire of 0.5 mm thickness as reference electrode with 1 M LiPF$_6$ in EC : DMC ratio 1:1 (LP30 Merck, Germany) as the electrolyte were polarised at $E = 0.10$ V for 6 h before measurement and left to equilibrate for 48 h. Measurements were taken at open circuit potential (OCP) in the temperature range from 285 to 305 K. The impedance spectra were obtained by applying a sinusoidal signal of 10 mV in amplitude in the frequency range from 100 kHz to 10 mHz.

Results and discussion

The X-ray diffraction pattern of thermally treated marine biomass is shown in Fig. 1. The XRD spectrum confirms the presence of crystobalite, quartz, traces of albite and magnetite.

The morphology of the carbonized biomass at different magnification (a) and (b) is illustrated by SEM images in Fig. 2. Regular square voids of 100 nm side length are seen for the material without milling. This is an example of a diatomic skeleton made of silica. The skeletons are of varied shape and their common feature is the presence of the holes.

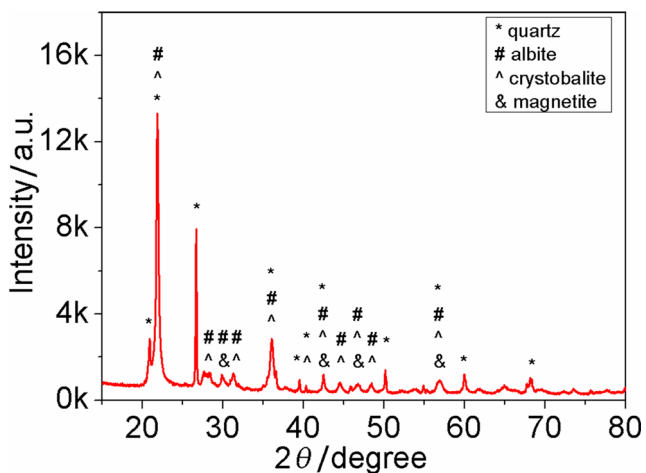These holes were expected to enhance the active surface area of the carbonized material as is required for
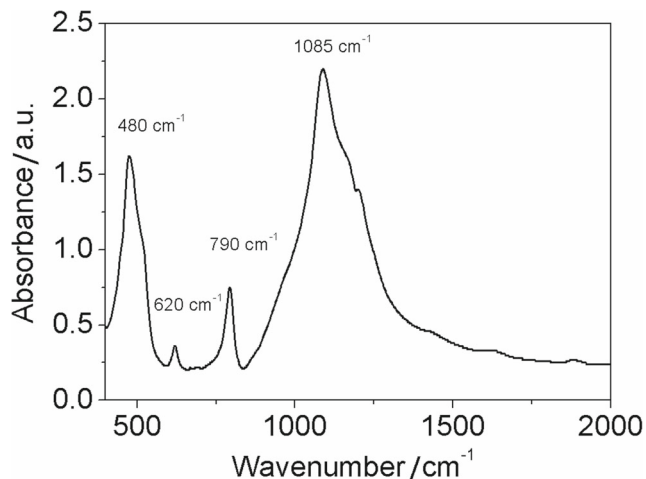
Fig. 1 XRD pattern of carbonized algae

Fig. 3 IR spectrum for carbonized biomass

nanomaterials for electrochemical application. Hence, the laborious preparation of a silica nanostructure is performed by nature, saving efforts in technological procedures and also saving energy consumption. After milling, the sample consists of rectangular shape, cubic-like particles of sizes up to about 5 μm. Crushing is expected to increase the active surface area required for a sufficient current outcome. However, Brunauer-Emmett-Teller (BET) nitrogen absorption/desorption analysis shows that the surface area of carbonized material is only 1.443 m^2 g^{-1} with a total pore volume of 0.0008 cm^3 g^{-1}. It evidences that carbonized material is rather compact with clearly visible nanovoids.

In the EDX spectrum, the presence of silicon, oxygen and other elements: potassium, calcium, magnesium, sodium, aluminium and iron was identified. The silicon content is 34 at.% while the amount of oxygen is at the level of 59 at.%. The amount of other elements is up to 7 at.%. They form

oxides (Fe) and, very likely, silicates (Al, Ca, K, Na, Mg); however, due to small amounts, only albite is recognized in the XRD pattern.

In Fig. 3, the absorption spectrum of thermally treated marine biomass has been presented.

As can be seen, the transversal optical (TO) resonance at 480 cm^{-1} is attributed to the rocking vibrational mode Si-O-Si, the O-Si-O bending mode at 790 cm^{-1} and the Si-O asymmetric stretching mode at 1080 cm^{-1} [17]. The signal at 620 cm^{-1} is attributed to stretching modes involving displacements associated primarily with the Si atom [21]. The presence of these peaks confirms that the material consists of silica particles.

Cyclic voltammetry (cv) curves for the first (red) and second (black) scan have been shown in Fig. 4.

The first scan discloses a clearly shaped cathodic maximum at 0.75 V. This peak is attributed to complex processes
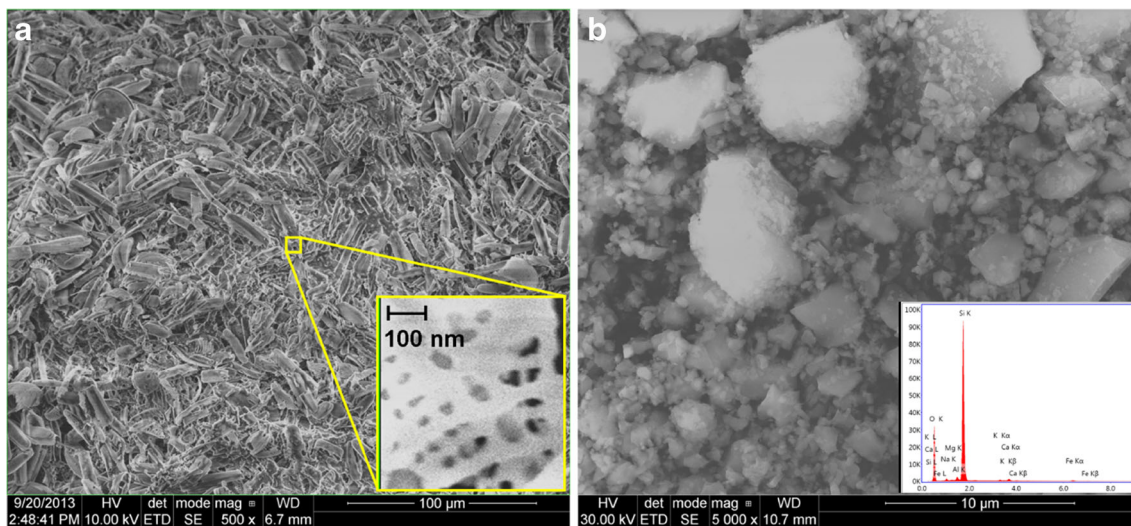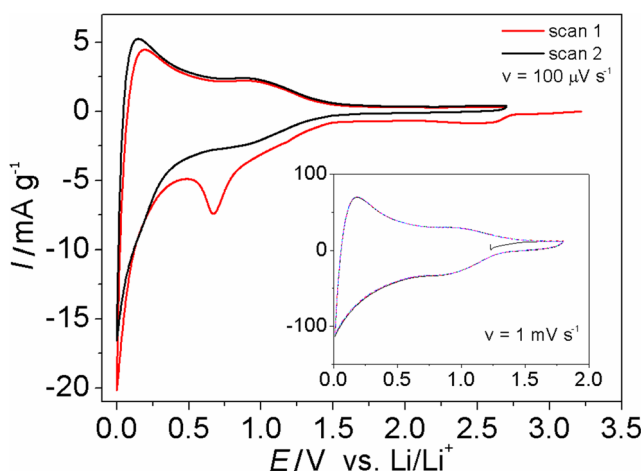

Fig. 2 SEM images of carbonized biomass. Before (**a**) and after (**b**) milling procedure. In the *inset*, the EDX analysis is given

Fig. 4 The first and second cv curve of an electrode covered with carbonized biomass. Sweep rate $100\,\mu V\,s^{-1}$. Potential range 0.005–3.0 V vs. Li/Li$^+$. *Inset*: 5 cycles ($v = 1$ mV s^{-1}) of lithium incorporation/exclusion from the electrode in potential range 0.005–1.8 V

Fig. 5 The complex plane impedance plot of carbonized biomass taken at different temperatures at potential $E = 0.1$ V (film thickness $\sim 40\,\mu m$, electrode surface area 1.2 cm^2)

of solid electrolyte formation at the interface (SEI) and electrochemical reduction of silica. Both these processes are parallel, taking part at the same potential range [8]. In the second scan, with no SEI formation, a current plateau starting from ~0.8 V has been recorded. The observed current growth corresponds to lithium silicate formation from SiO$_2$ [16, 40]. This reduction may proceed according to reaction (1) or (3) (see Introduction) and in all possible cases silicon is created as a reduction product. In our previous study on anode material made from biomass, it was proven by XPS measurements that lithiation of diatomic silica leads to formation of lithium silicates (Li$_x$SiO$_y$) and lithium silicide Li$_x$Si [23].

At lower potentials, alloy Li$_x$Si formation [40] and lithium insertion into added carbon black may occur [28]. Silicon, the reduction product, should be dispersed in the bulk of the electrode material in a way that alloying formation and its volume changes would be compensated by the porous material structure. In the inset, multicyclic (fast) cv curves of the electrode material after charging/discharging steps (see Fig. 4) have been shown. The curves overlap, indicating that the material is stable during the cycling procedure and exhibit coulombic efficiency above 99.1% for the fifth cycle.

The impedance spectra at potential $E = 0.1$ V and taken at different temperatures are presented in Fig. 5.

The EIS spectra consist of two depressed semicircles at higher and medium frequencies, followed by a straight line rising at an angle of 80° to the Z′ axis. The first semicircle is attributed to the SEI response [37]. The second semicircle is well shaped at the middle range of frequencies. The almost vertical line at lower frequencies is observed which may indicate a finite-length diffusional impedance to the
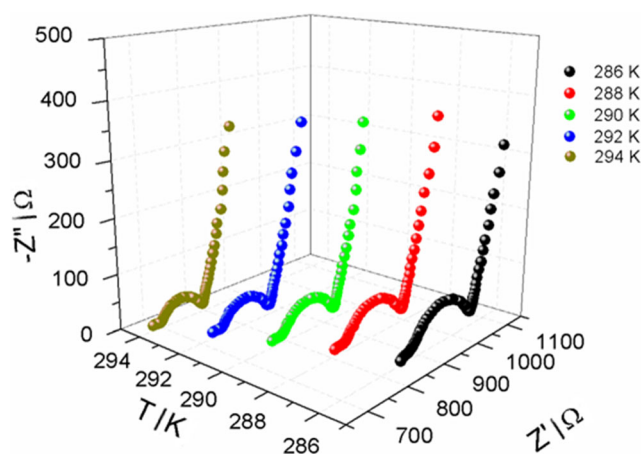
blocking electrode [11]. Thus, Warburg element Z_W is replaced by the generalised finite-length Warburg element (Z_{GFW}) as it is given in Ref. [25, 36].

The EIS data were analysed using an electric equivalent circuit (EEC) presented in the inset in Fig. 6a.

The EEC is a modified Randles equivalent circuit connected in series with (RC) elements responding to SEI impedance. The meaning of symbols is as follows: R_e is the electrolyte resistance, CPE_{SEI} and R_{SEI} are attributed to SEI capacitance and SEI film resistance, CPE_{ct} and R_{ct} are double layer capacitance and charge transfer resistance from SEI to a bulk film, Z_{GFW} is finite-length diffusional impedance including inhomogeneity of the electrode as is given in Ref. [36]. The goodness of fit (χ^2) was in the range $1\ 10^{-5} \div 1\ 10^{-6}$ indicating that the proposed EEC is acceptable.

The impedance plots of charged material ($E = 0.1$ V) and pristine electrode material ($E = 3.0$ V) are shown in Fig. 6a, b, respectively. The impedance of a freshly prepared electrode in contact with an aprotic electrolyte is low. The shape of the impedance spectrum taken for a freshly prepared electrode in contact with a non-aqueous electrolyte is similar to impedance functions obtained for porous electrodes. It is known that the type of pores may affect the impedance response as shown in Ref. [19, 24]. In the inset in Fig. 2a, one may see that diatoms belong to porous material group [31] with various types of nanopores. Due to these features, one may use them as an electrode material enabling faradaic reaction of the nanoporous biosilica-electrode to occur.

Impedance of the material increases after charging and two separate arcs of different time constants are clearly distinguishable. A constant phase element (CPE) has been applied in the electrical equivalent circuit in both parts of

Fig. 6 Nyquist plot for **a** carbonized biomass (O) at $E = 0.1$ V with fitting results (X) obtained using electric equivalent circuit presented in the inset and **b** pristine electrode material (thickness ∼40 μm, electrode surface area 1.2 cm^2)
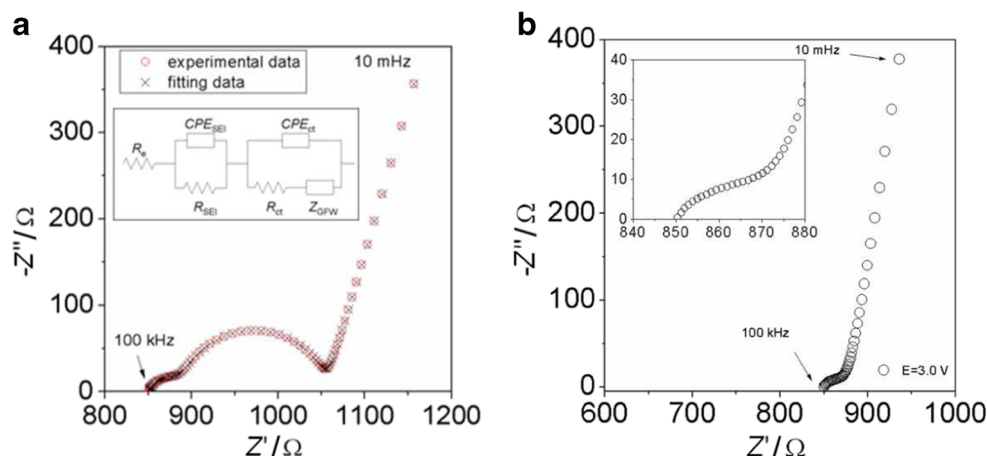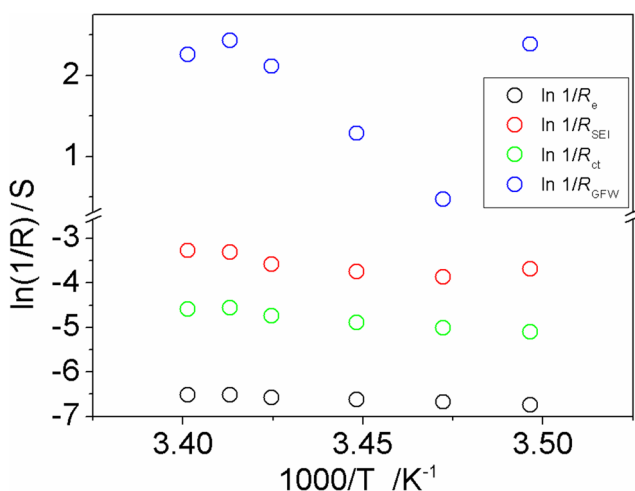

EEC. From definition, the CPE is characterised by two parameters: Q and n. When $n = 0$ then CPE represents resistance, capacitance for $n = 1$ and a Warburg impedance when $n = 0.5$ [43]. The general formula of the CPE is [2]:

$$Z(\omega) = \frac{1}{Q}(j\omega)^{-n} \tag{5}$$

Here, $j = \sqrt{-1}$, n is a non-dimensional exponent changing in the range $0 < n < 1$, and Q is a constant of dimension $F\ s^{n-1}$.

The generalised finite-length Warburg element (Z_{GFW}) is characterised by resistance R_{GFW}, time constant T_c and an exponent θ. The Z_{GFW} element variation of the heuristically modified CPE and Warburg diffusion expression in one formula arises from non-uniform diffusion in a finite-length region; here, that function has been implemented for the studied non-homogenous material according to Ref. [25, 36]:

$$Z_{GFW} = \frac{R_{GFW}}{(j\omega T_c)^\theta}\tanh[(j\omega T_c)^\theta] \tag{6}$$
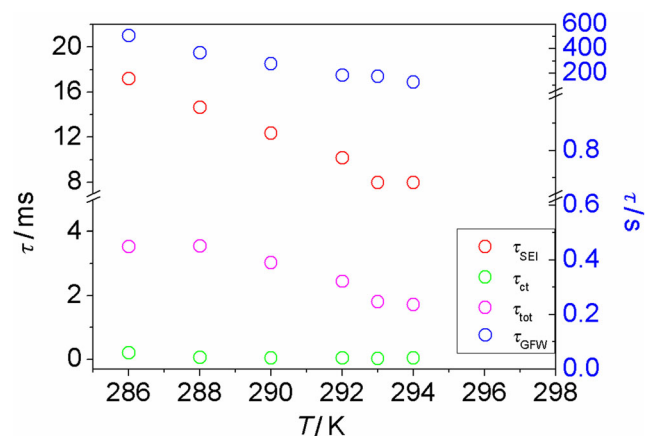
The term *non-uniform* is due to the complexity of the biomaterial. It is not only diffusion within carbonaceous material but also the diffusion in the inorganic part coming from diatoms biosilica. This inhomogeneity leads to the diffusion process in not uniform material expressed by Eq. 6 representing generalised finite-length Warburg impedance.

In Fig. 7, the temperature dependence of $\ln(\frac{1}{R}) = f(\frac{1}{T})$ has been presented.

The $\ln\frac{1}{R}$ fulfils the Arrhenius type temperature dependence for electrolyte, SEI and charge transfer resistances. Conductivity increases with temperature. However, the resistance of the film R_{GFW} is not temperature-dependent in studied temperature range. This resistance is attributed to bulk film. Similar behaviour was observed for metal hexacyanoferrate, zeolite type systems penetrated by counter ions as was shown in Ref. [15, 22].

In Fig. 8, the time constant (τ) values have been shown. The time constant was calculated by the equation given below [34]:

$$CPE = \frac{\tau^n}{R} \tag{7}$$

Fig. 7 Plot of $\ln(\frac{1}{R}) = f(\frac{1}{T})$ for carbonized biomass at potential $E = 0.1$ V

Fig. 8 The time constant against temperature for carbonized biomass

Fig. 9 Parameter values obtained from fitting the experimental impedance spectra of a carbonized algae electrode at different temperatures. **a** CPE_{SEI-C} and **b** CPE_{ct-C}
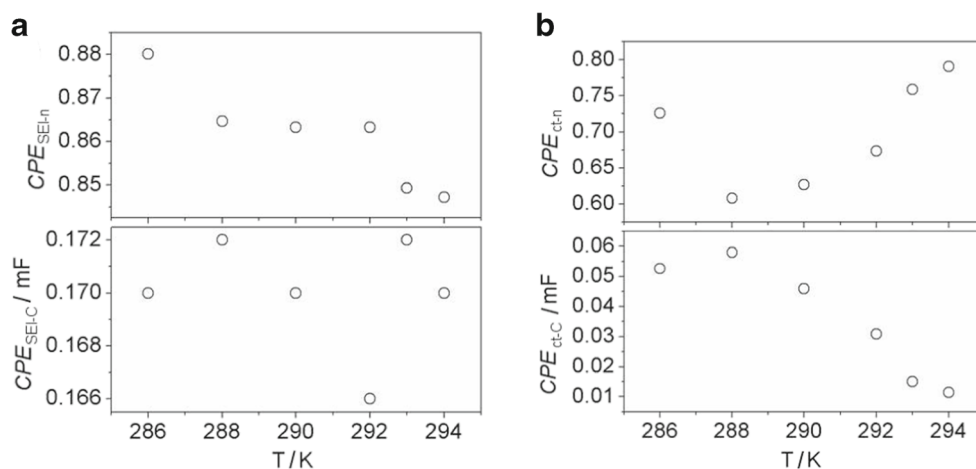
The time constant is a value which may be considered as the time taken for the electrode material to be charged/discharged in terms of capacitor/galvanic cell behaviour. It is commonly used for electrochemical applications [1, 3, 7, 41]. In general, it gives information about charge and discharge processes taking place in the entire system, i.e. a double electrochemical layer in the metal/bulk film interface, within particles in the bulk film and the metal/electrolyte interface. This is the inverse angular frequency at the maximum of the conductivity arc [13].

The average time of τ_{tot} is 2.67 10^{-3} s. It suggests that charge transfer is fast and might be dependent on coupled lithium ion and electron processes in the studied system. A similar value of the time constant was calculated by Novák et al. for commercially available graphite [20].

The results show that the relaxation time in SEI films diminishes with temperature increase and is lower for T = 294 K and the fastest for T = 286 K and equal to 0.00796 and 0.017 s, respectively. Similar behaviour was observed for τ_{SEI} calculated for charge transfer from SEI to the bulk material. The time constant values of τ_{ct} were of two orders of magnitude lower in comparison with τ_{SEI}. It shows that the charge transfer process of SEI interface/silica particles is faster than charge transfer within the SEI film.

The time constant value calculated from the Z_{GFW} element is in the range 125–500 s. This order of magnitude confirms that the diffusion process of lithium ions in the bulk material is very slow. Thus, one may conclude that diffusion is the limiting step of the electrode reaction. To calculate pseudocapacitance (CPE_C) from the constant phase element, we used the equation given by Brug et al. [4]:

$$CPE_C = Q^{\frac{1}{n}} \cdot R^{(1-n)/n} \tag{8}$$

where R is the resistance, Q is a constant proportional to the active area and n describes *capacitance distribution* (it changes in the range $0 < n < 1$).

In Fig. 9 the constant phase element vs. temperature relation has been presented.

The pseudocapacitance (CPE_{SEI-C}) of the SEI film is almost constant with temperature, while (CPE_{SEI-n}) slightly decreases. The CPE_{SEI-n} is an exponential parameter which shows the non-ideal behaviour of the system. The values of those parameters may suggest that the SEI interface does not grow at the studied potential. SEI film homogeneity has an impact on the charge transfer reaction taking place at the SEI interface and silica particles. As can be seen in Fig. 9b, in the temperature range from 288 to 294 K, CPE_{ct-C} values decrease while CPE_{ct-n} increase. The change of these parameters may reflect the change of inhomogeneity of the charge transfer reaction induced by the formed SEI film.

The data on the change of capacity depending on the applied current and the number of cycles have been shown in Fig. 10.

The charge capacity of carbonized biomass for the first lithium insertion is 1490 mAh g^{-1}, while the first extraction
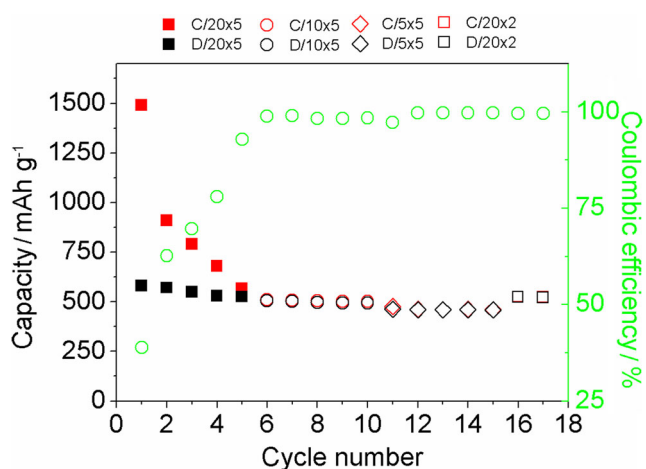
Fig. 10 The capacity vs. cycle number of carbonized biomass at different C-rates

capacity is 580 mAh g^{-1}. It gives an irreversible capacity loss of 61%. Such high capacity loss is very likely attributed to irreversible reactions resulting with lithium silicate and/or lithium oxide formation. High irreversible capacity should be reduced for practical applications. There might be several ways to decrease capacity loss. One is to change size of the particles. According to Gao et al., commercial silica of 7 nm diameter gives a reversible capacity of 400 mAh g^{-1} [14]. The other possibility is to add additives to obtain a stable solid electrolyte interphase (SEI). A stable SEI layer prevents electrolyte decomposition and lithium loss. It might be done by the following: (1) additive addition to electrolyte, i.e. vinylene carbonate (VC), tris(pentafluorophenyl) borane (TPFPB)) or (2) chemical modification of the silica surface by a group of alkoxy silane additives (trimethoxymethylsilane, dimethoxydimethylsilane, methoxytrimethylsilane) [42]. Capacity loss may be also decreased by electrode material prelithiation using ex situ electrochemical and chemical methods [10, 27]. The capacity retention for C/20, C/10 and C/5-rates after 5 cycles is 17, 30 and 67%, respectively. However, capacity fading for the next two C/20 – rates is only 2.7% with the final charge capacity equal to 521 mAh g^{-1}. The electrochemical reduction with formation of irreversible products is required for further stable charging/discharging behaviour.

Conclusions

The material obtained by pyrolysis of marine algae contains porous silica. Silica is present in the form of rectangular shaped particles of different kinds of crystallographic types. Crystobalite, quartz and a small amount of albite and magnetite have been identified by means of the XRD technique. Infrared spectroscopy evidences the Si-O vibrations coming from SiO_2.

Impedance spectra at potential $E = 0.1$ V performed at different temperatures show the presence of two depressed semicircles followed by a sloping line. The presence of depressed semicircles, in the form of constant phase elements instead of pure capacitors in the electric equivalent circuit, indicates that the material is porous, inhomogeneous and that the surface is rough.

Electrochemical processes occurring in the SEI film and between SEI interface/silica particles have been identified. The diffusion of Li-ion has been modelled with the generalised finite-length Warburg element instead of a finite Warburg element. The time constant of SEI film impedance is 10^4 lower in comparison with the time constant originating from modified Randles circuit values related to the charge transfer process between the SEI interface and silica particles. Lithium-ion diffusion in the bulk film is the slowest process. The pseudocapacitance of the SEI film is

constant and is not temperature-dependent but influences the charge transfer capacitance.

The presence of the silica nanostructure enhances cycle stability in that natural material. However, it is still a challenge with the reproducibility of the material. We are aware that the presence of crystobalite, quartz, traces of albite and magnetite might differ if one goes from batch to batch. More detailed studies are required to give an answer to that problem. Nevertheless, the results show that naturally occurring, renewable source of nanoporous silica from sea water diatoms are found to be suitable as the anode material for lithium-ion battery applications with a higher specific charge capacity than graphite and similar time constants for the lithiation process.

References

1. Aurbach D, Zaban A (1994) Impedance spectroscopy of lithium electrodes: part 3. The importance of Li electrode surface preparaion. J Electroanal Chem 365:41–45
2. Bisquert J, Garcia-Belmonte G, Bueno P, Longo E, Bulho LOS (1998) Impedance of constant phase element (CPE)-blocked diffusion in film electrodes. J Electroanal Chem 452:229–234
3. Bruce PG, Scrosati B, Tarascon JM (2008) Nanomaterials for rechargeable lithium batteries. Angew Chem 47(16):2930–46
4. Brug G, van den Eeden A, Sluyters-Rehbach M, Sluyters J (1984) The analysis of electrode impedances complicated by the presence of a constant phase element. J Electroanal Chem 176:275–295
5. Chang WS, Park CM, Kim JH, Kim YU, Jeong G, Sohn HJ (2012) Quartz (SiO_2): a new energy storage anode material for Li-ion batteries. Energy Environ Sci 5(5):6895–6899
6. Chen Y, Nie M, Lucht BL, Saha A, Guduru PR, Bose A (2014) High capacity, stable silicon/carbon anodes for lithium-ion batteries prepared using emulsion-templated directed assembly. ACS Appl Mater Interfaces 6(7):4678–4683
7. Dees DW, Kawauchi S, Abraham DP, Prakash J (2009) Analysis of the Galvanostatic Intermittent Titration Technique (GITT) as applied to a lithium-ion porous electrode. J Power Sources 189(1):263–268
8. Dimov N, Kugino S, Yoshio M (2003) Carbon-coated silicon as anode material for lithium ion batteries: advantages and limitations. Electrochim Acta 48(11):1579–1587
9. Doh CH, Veluchamy A, Lee DJ, Lee JH, Jin BS, Moon SI, Park CW, Kim DW (2010) Comparative study on performances of composite anodes of SiO, Si and Graphite for lithium rechargeable batteries. Bull Korean Chem Soc 31(5):1257–1261
10. Forney MW, Ganter MJ, Staub JW, Ridgley RD, Landi BJ (2013) Prelithiation of silicon carbon nanotube anodes for lithium ion

batteries by stabilized lithium metal powder (SLMP). Nano Lett 13:4158–4163

11. Funabiki A, Ogumi Z (1998) Impedance study on the electrochemical lithium intercalation into natural graphite powder. J Electrochem Soc 145(1):172–178

12. Funabiki A, Inaba M, Ogumi Z (1997) A.C. Impedance analysis of electrochemical lithium intercalation into highly oriented pyrolytic graphite. J Power Sources 68:227–231

13. Funke K (2013) Solid state ionics: from Michael Faraday to green energy—the European dimension. Sci Technol Adv Mater 14(4):043,502

14. Gao B, Sinha S, Fleming L, Zhou O (2001) Alloy formation in nanostructured silicon. Adv Mater 11:816–819

15. Garcia-Jareno J, Sanmatias A, Vicente F, Benito D (1998) Temperature dependence of impedance spectra of pRussian Blue films deposited on IT0 electrodes. Electrochim Acta 43(97):235–243

16. Guo B, Shu J, Wang Z, Yang H, Shi L, Liu Y, Chen L (2008) Electrochemical reduction of nano-SiO_2 in hard carbon as anode material for lithium ion batteries. Electrochem Commun 10:1876–1878

17. Hu Q, Suzuki H, Gao H, Araki H, Yang W, Noda T (2003) High-frequency FTIR absorption of SiO_2/Si nanowires. Chem Phys Lett 378(3-4):299–304

18. Kaspar J, Graczyk-Zajac M, Riedel R (2014) Determination of the chemical diffusion coefficient of Li-ions in carbon-rich silicon oxycarbide anodes by electro-analytical methods. Electrochim Acta 115:665–670

19. Keiser H, Beccu KD, Gutjahr MA (1976) Abschtzung der porenstruktur porser elektroden aus impedanzmessungen. Electrochim Acta 21:539–543

20. La Mantia F, Vetter J, Novák P (2008) Impedance spectroscopy on porous materials: a general model and application to graphite electrodes of lithium-ion batteries. Electrochim Acta 53(12):4109–4121

21. Lippincott ER, Valkenburg AV, Weir CE, Bunting EN (1958) Infrared studies on polymorphs of silicon dioxide and germanium dioxide. J Res Natl Bur Stand 61(1):61–70

22. Lisowska-Oleksiak A, Nowak AP (2008) Impedance spectroscopy studies on hybrid materials consisting of poly(3,4-ethylenedioxythiophene) and iron, cobalt and nickel hexacyanoferrate. Solid State Ion 179(1-6):72–78

23. Lisowska-Oleksiak A, Nowak AP, Wicikowska B (2014) Aquatic biomass containing porous silica as an anode for lithium ion batteries. RSC Adv 4:40,439–40,443

24. Macdonald DD (2006) Reflections on the history of electrochemical impedance spectroscopy. Electrochim Acta 51:1376–1388

25. MacDonald J, Johnson MB (1987) Impedance spectroscopy: emphasizing solid materials and systems. Wiley-Vch, New York

26. NuLi Y, Yang J, Jiang Z (2006) Intercalation of lithium ions into bulk and powder highly oriented pyrolytic graphite. J Phys Chem Solid 67(4):882–886

27. Pan Q, Zuo P, Mu T, Du C, Cheng X, Ma Y (2017) Improved electrochemical performance of micro-sized SiO-based composite anode by prelithiation of stabilized lithium metal powder. J Power Sources 347:170–177

28. Pistoia G (1994) Lithium batteries: new materials, developments, and perspectives

29. Reddy MV, Subba Rao GV, Chowdari BVR (2013) Metal oxides and oxysalts as anode materials for Li ion batteries. Chem Rev 113(7):5364–457

30. Ruffo R, Hong SS, Chan CK, Huggins RA, Cui Y (2009) Impedance analysis of silicon nanowire lithium ion battery anodes. J Power Sources 189(2):11,390–11,398

31. Seethalakshmi N, Selvakumar R (2015) Investigation of porous silica nanostructures in diatoms isolated from Kurichi and Sulur lakes of Coimbatore, India using field emission scanning electron microscopy. Micron 79:24–28

32. Seong IW, Kim KT, Yoon WY (2009) Electrochemical behavior of a lithium-pre-doped carbon-coated silicon monoxide anode cell. J Power Sources 189(1):511–514

33. Teki R, Datta MK, Krishnan R, Parker TC, Lu TM, Kumta PN, Koratkar N (2009) Nanostructured silicon anodes for lithium ion rechargeable batteries. Small 5(20):2236–42

34. Turcio-Ortega D, Pandiyan T, García-Ochoa EM (2007) Electrochemical impedance spectroscopy (EIS) study of the film formation of 2-imidazoline derivatives on carbon steel in acid solution. Mater Sci 13(2):163–166

35. Umeda M, Dokko K, Fujita Y, Mohamedi M, Uchida I, Selman JR (2001) Electrochemical impedance study of Li-ion insertion into mesocarbon microbead single particle electrode: part I. Graphitized carbon. Electrochim Acta 47:885–890

36. Wang C, Appleby AJ, Little FE (2001) Electrochemical impedance study of initial lithium ion intercalation into graphite powders. Electrochim Acta 46:1793–1813

37. Wang C, Appleby AJ, Little FE (2002) Irreversible capacities of graphite anode for lithium-ion batteries. J Electroanal Chem 519:9–17

38. Wang K, Ma B, Wang Y, An L (2013) Complex impedance spectra of Polymer-Derived silicon oxycarbides. J Am Ceram Soc 96(5):1363–1365

39. Winter BM, Besenhard JO, Spahr ME, Novak P (1998) Insertion electrode materials for rechargeable lithium batteries. Adv Mater (10):725–763

40. Yan N, Wang F, Zhong H, Li Y, Wang Y, Hu L, Chen Q (2013) Hollow porous SiO_2 nanocubes towards high-performance anodes for lithium-ion batteries. Sci Rep 3:1568–1574

41. Yu P, Popov BN, Ritter JA, White RE (1999) Determination of the lithium ion diffusion coefficient in graphite. J Electrochem Soc 146(1):8–14

42. Zhang S, He M, Su CC, Zhang Z (2016) Advanced electrolyte/additive for lithium-ion batteries with silicon anode. Curr Opin Chem Eng 13:24–35

43. Zoltowski P (1998) On the electrical capacitance of interfaces exhibiting constant phase element behaviour. J Electroanal Chem 443(1):149–154